NASA/TM–2015-218967

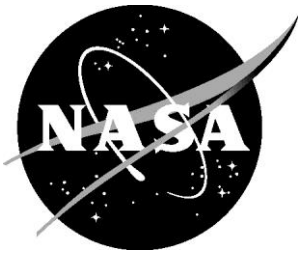

Test and Analysis Correlation for a Y-Joint Specimen for a Composite Cryotank

Brian H. Mason, David W. Sleight, and Ray W. Grenoble
Langley Research Center, Hampton, Virginia

October 2015

NASA STI Program . . . in Profile

Since its founding, NASA has been dedicated to the advancement of aeronautics and space science. The NASA scientific and technical information (STI) program plays a key part in helping NASA maintain this important role.

The NASA STI program operates under the auspices of the Agency Chief Information Officer. It collects, organizes, provides for archiving, and disseminates NASA's STI. The NASA STI program provides access to the NTRS Registered and its public interface, the NASA Technical Reports Server, thus providing one of the largest collections of aeronautical and space science STI in the world. Results are published in both non-NASA channels and by NASA in the NASA STI Report Series, which includes the following report types:

- TECHNICAL PUBLICATION. Reports of completed research or a major significant phase of research that present the results of NASA Programs and include extensive data or theoretical analysis. Includes compilations of significant scientific and technical data and information deemed to be of continuing reference value. NASA counter-part of peer-reviewed formal professional papers but has less stringent limitations on manuscript length and extent of graphic presentations.

- TECHNICAL MEMORANDUM. Scientific and technical findings that are preliminary or of specialized interest, e.g., quick release reports, working papers, and bibliographies that contain minimal annotation. Does not contain extensive analysis.

- CONTRACTOR REPORT. Scientific and technical findings by NASA-sponsored contractors and grantees.

- CONFERENCE PUBLICATION. Collected papers from scientific and technical conferences, symposia, seminars, or other meetings sponsored or co-sponsored by NASA.

- SPECIAL PUBLICATION. Scientific, technical, or historical information from NASA programs, projects, and missions, often concerned with subjects having substantial public interest.

- TECHNICAL TRANSLATION. English-language translations of foreign scientific and technical material pertinent to NASA's mission.

Specialized services also include organizing and publishing research results, distributing specialized research announcements and feeds, providing information desk and personal search support, and enabling data exchange services.

For more information about the NASA STI program, see the following:

- Access the NASA STI program home page at http://www.sti.nasa.gov

- E-mail your question to help@sti.nasa.gov

- Phone the NASA STI Information Desk at 757-864-9658

- Write to:
  NASA STI Information Desk
  Mail Stop 148
  NASA Langley Research Center
  Hampton, VA 23681-2199

NASA/TM–2015-218967

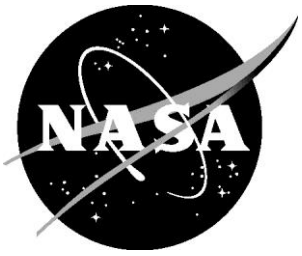

Test and Analysis Correlation for a Y-Joint Specimen for a Composite Cryotank

Brian H. Mason, David W. Sleight, and Ray W. Grenoble
Langley Research Center, Hampton, Virginia

National Aeronautics and
Space Administration

Langley Research Center
Hampton, Virginia 23681-2199

October 2015

Available from:

NASA STI Program / Mail Stop 148
NASA Langley Research Center
Hampton, VA 23681-2199
Fax: 757-864-6500

Test and Analysis Correlation for a Y-Joint Specimen for a Composite Cryotank

Brian H. Mason*, David W. Sleight†, and Ray Grenoble‡
NASA Langley Research Center, Hampton, VA, 23681-2199

The Composite Cryotank Technology Demonstration (CCTD) project under NASA's Game Changing Development Program (GCDP) developed space technologies using advanced composite materials. Under CCTD, NASA funded the Boeing Company to design and test a number of element-level joint specimens as a precursor to a 2.4-m diameter composite cryotank. Preliminary analyses indicated that the y-joint in the cryotank had low margins of safety; hence the y-joint was considered to be a critical design region. The y-joint design includes a softening strip wedge to reduce localized shear stresses at the skirt/dome interface. In this paper, NASA-developed analytical models will be correlated with the experimental results of a series of positive-peel y-joint specimens from Boeing tests. Initial analytical models over-predicted the experimental strain gage readings in the far-field region by approximately 10%. The over-prediction was attributed to uncertainty in the elastic properties of the laminate and a mismatch between the thermal expansion of the strain gages and the laminate. The elastic properties of the analytical model were adjusted to account for the strain gage differences. The experimental strain gages also indicated a large non-linear effect in the softening strip region that was not predicted by the analytical model. This non-linear effect was attributed to delamination initiating in the softening strip region at below 20% of the failure load for the specimen. Because the specimen was contained in a thermally insulated box during cryogenic testing to failure, delamination initiation and progression was not visualized during the test. Several possible failure initiation locations were investigated, and a most likely failure scenario was determined that correlated well with the experimental data. The most likely failure scenario corresponded to damage initiating in the softening strip and delamination extending to the grips at final failure.

I. Introduction

A. Motivation and Background

NASA is currently developing the next generation of launch vehicles to perform asteroid investigation and other interplanetary missions. A crucial component of these missions is the use of lower weight advanced materials in various structural components of the launch vehicles, including the liquid hydrogen (LH_2) cryogenic tanks (cryotanks). NASA's Game Changing Development Program (GCDP) in the Space Technology Mission Directorate (STMD) is tasked with maturing advanced space technologies that may lead to new approaches for future space missions and transfer of these technologies to other government and industrial entities. The Composite Cryotank Technology Demonstration (CCTD) Project was a part of the GCDP and was responsible for development of space technologies utilizing advanced composite materials (see Refs. 1 and 2).

During 2012 and 2013, NASA and its industry partner, Boeing, participated in Phase II of the CCTD Project to design, manufacture, and test a 2.4-m diameter precursor cryotank. In 2014, a 5.5-m diameter test article cryotank was designed, manufactured, and tested based on lessons learned from the precursor cryotank. At present, testing of the precursor tank is complete, and design and manufacturing of the 5.5-m cryotank has been completed. One of the element-level test specimens developed for the precursor tank is a positive peel y-joint specimen, shown in Figure 1. This specimen was developed because analyses from Phase I of the CCTD Project indicated that the y-joint region had low margins of safety, and hence, the performance of this joint was critical to the cryotank design. Several y-joint specimens were tested by Boeing in September 2012, but a detailed study of the failure modes of the specimens could not be completed prior to testing of the precursor tank due to the project schedule. In this paper, the failure

*Research Aerospace Engineer, Durability, Damage Tolerance, and Reliability Branch, Senior Member AIAA
†Research Aerospace Engineer, Structural and Thermal Systems Branch, Senior Member AIAA
‡Research Aerospace Engineer, Durability, Damage Tolerance, and Reliability Branch, Senior Member AIAA

modes of the y-joint specimens are investigated. Results from this y-joint study were used to help establish modeling and analysis methods for use in evaluation of the design for the 5.5-m diameter cryotank.

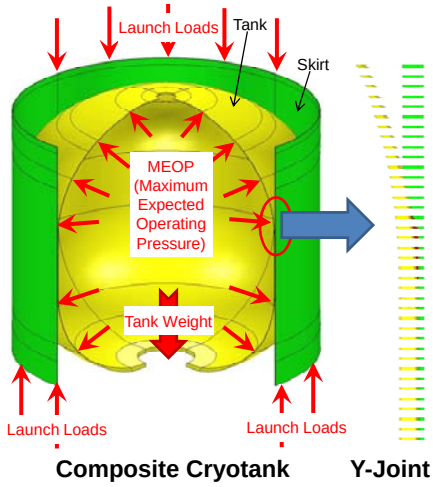

Figure 1. Exploded view of cryotank and y-joint.

B. Purpose and Contents

The purpose of this paper is to correlate structural analysis models of the y-joint test specimens with the failure modes and strains observed during test. Due to the very tight schedule of the CCTD Project, only coarse models of the specimens were completed prior to the test. Stresses in the coarse model were obtained for the applied failure load for use as design allowables for the tank, but the strains in the coarse model were never evaluated against the test strain gage values. The detailed structural models of the y-joint were completed soon after the tests, but due to schedule issues, they could not be adjusted to correlate with the strain gage data until after the tests on the precursor tank were completed. In this paper, the process of correlating the detailed models with the composite delamination failure mode observed during the y-joint specimen tests is discussed. This approach illustrates the issues associated with proceeding to larger scale design and test without first understanding the failure modes of simpler element-level specimens.

This paper is organized as follows. Section II provides a description of the y-joint test specimen, the test setup, and the analysis models. Section III presents the approach used to correlate the analysis models with the test. Section IV presents the results of a linear elastic fracture mechanics analysis of the y-joint model. A summary of the approach used in the paper and the conclusions of the study are presented in Section V.

II. Model Geometry and Loads

In this section, the y-joint structural analysis problem is described. The test specimen geometry and key structural features are described first. Next, the finite element (FE) model and the analyses that simulate the y-joint and its response are discussed. In the third part of this section, experimental tests performed in September 2012 are described.

A. Test Specimen

The y-joint specimen consists of a flat composite coupon 24 in. long by 2.5 in. wide, representing the dome of the tank pressure vessel, as shown in Figure 2. Two panels representing the skirt of the tank are bonded to either side of the dome simulator section, making the model symmetric. The skirt simulator consists of a flat section 17.17 in. long with a 3.13 in. angled section. A triangular softening strip is bonded in the angled gap between the skirt and the dome. The specimen was tested under an applied tensile axial load (P) at cryogenic conditions. Loading on the specimen is intended to simulate the pressure load on the tank (tank stress = P R/2t). Note that neither hoop stresses, axial launch loads, nor gravity loads are represented in this test configuration.

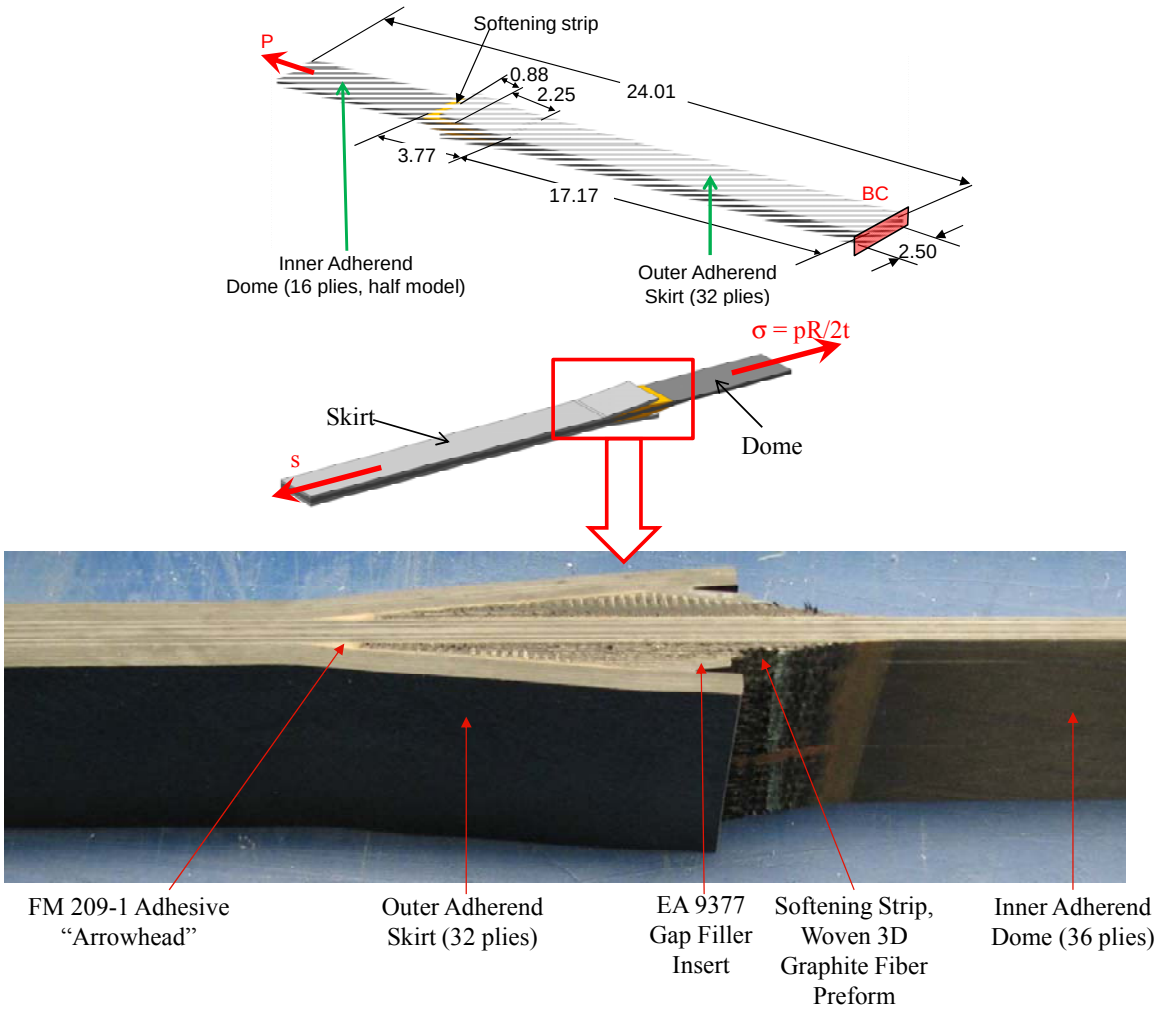

Figure 2. Geometry of the positive peel y-joint specimen**.**

The inner adherend (dome) laminate consists of 36 plies of IM7/5320-1 tape as shown in Figure 2. Note that the thickness of the inner adherend is double the thickness of the actual dome, although the stacking sequence is identical. The outer adherend (skirt) laminate is 32 plies of IM7/5320-1. The outer adherend is bonded to the inner adherend with FM209-1M film adhesive. The softening strip is a woven 3D graphite fiber preform infused with a fluorinated ethylene propylene (FEP) matrix. The softening strip is used to reduce localized shear stresses at the skirt/dome interface as shown in Figure 3 (Ref. 2). A gap filler (EA 9377) insert is attached at the softening strip/outer adherend interface. The gap filler is part of the insulation barrier for testing of the full tank. Because a statistically significant number of strength characterization tests for the unidirectional IM7/5320-1 material system were not performed, material strength data for the IM7/5320-1 tape are not available.

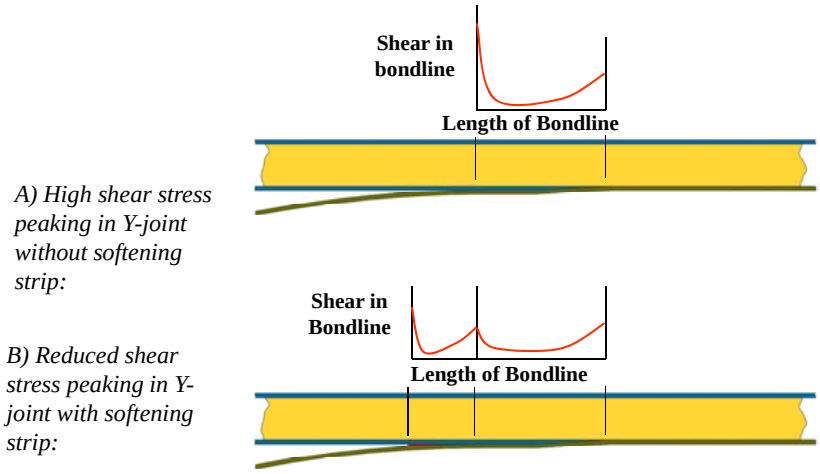

Figure 3. Shear stress distribution for y-joint A) without softening strip and B) with softening strip

B. Experimental Test Configuration and Results

To protect the proprietary nature of the test, only the basic details of the test are described in this paper. For the tests presented in this study, three specimens were cut from a larger skirt/dome panel that was cured out of autoclave (OoA).

For testing, the specimen is encased in a thermally insulated box as shown in Figure 4; therefore, the specimens were not visible during testing. During the test, the specimen is cooled down to -423°F using cryogenic hydrogen. After the temperature is stabilized at -423°F, the strain gage readings are reset to zero. The specimen is then loaded in tension until failure. In this paper, the three tests conducted in September 2012 are labeled PPY-1-A, PPY-1-B, and PPY-1-C where PPY means positive peel y-joint.

Figure 4. Test specimen encased in thermal insulation box.

One of the failed test specimens is shown in Figure 5. The specimen delaminated in the outermost plies of the inner adherend. The delamination extends from a tear in the softening strip to the grips of the specimen. The delamination is symmetric in nature. Initiation of the delamination was not directly observed because specimens were not visible during testing.

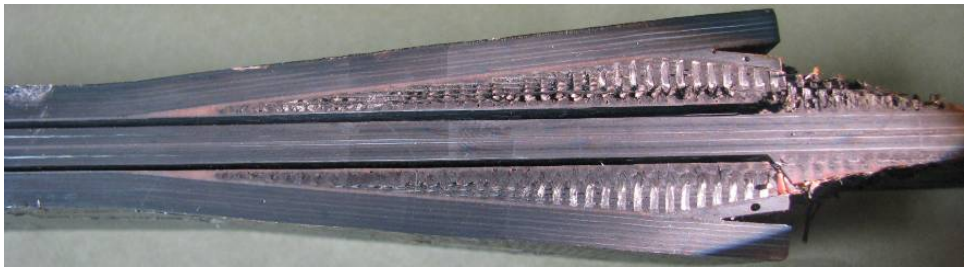

Figure 5. Failed test specimen.

C. Analysis Models

All FE analyses are performed with the ABAQUS software, a product of Simulia (Ref. 3)[§]. The FE model of the specimen consists mostly of 8-node solid hexahedral continuum elements (C3D8I) with a few 6-node solid wedge continuum elements (C3D6) in the arrowhead adhesive region. Several FE models were generated with different mesh discretizations and crack initiation locations, as discussed below.

Model 1 is illustrated in Figure 6. Model 1 consists of 1,063,351 elements and 1,175,377 nodes. A lateral mesh aspect ratio of 4.6 is used throughout the model. The mesh aspect ratio in the axial direction is 4.6 in the vicinity of the softening strip and 18.3 in the far-field region. Several mesh size studies were conducted, and the large far-field mesh size was deemed to be adequate because the model is in tension (with no bending) in the far-field regions. Each of the outermost 8 plies of the inner adherend and the innermost 12 plies of the outer adherend are modeled with one element through-the-thickness. The remaining 10 plies in the inner adherend and 24 plies in the outer adherend are modeled with two and four elements through-the-thickness, respectively. Symmetry boundary conditions are applied along the centerline of the inner adherend (labeled "C/L" in Figure 6).

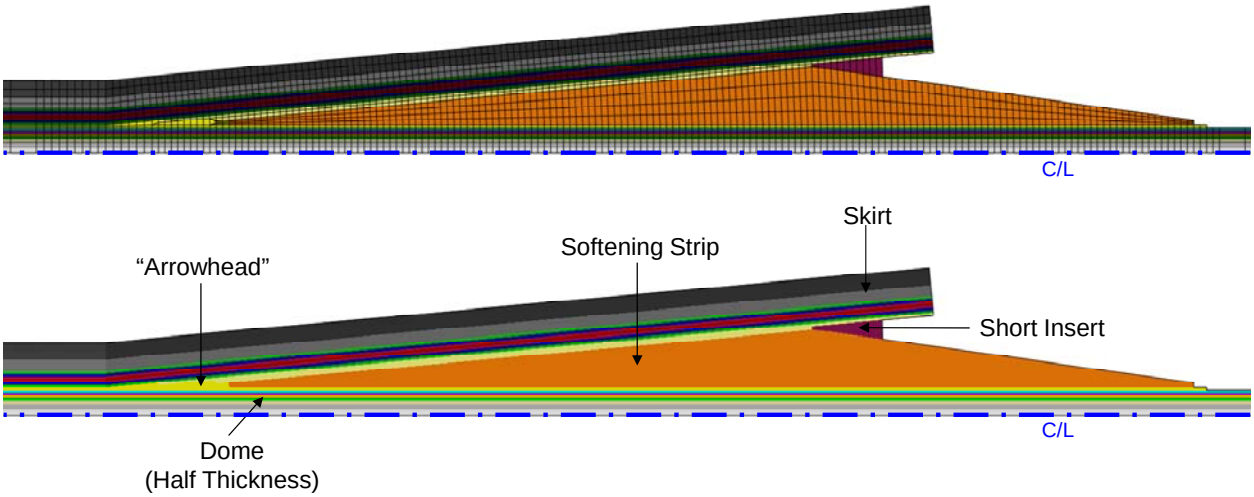

Figure 6. Model 1.

Model 2 is illustrated in Figure 7. Model 2 consists of 761,110 elements and 863,175 nodes. The lateral mesh aspect ratio is 1.8 at the free edges and 11.0 in the middle. The mesh aspect ratio in the axial direction is 1.1in the vicinity of the softening strip damage, 4.6 in the rest of the softening strip, and 18.3 in the far-field region. The through-the-thickness mesh density and symmetric boundary conditions are identical to Model 1. Geometrically, model 2 represents damage to the softening strip with a missing vertical strip of elements in the softening strip immediately beyond the gap filler insert.

[§] The use of trademarks or names of manufacturers in this report is for accurate reporting and does not constitute an official endorsement, either expressed or implied, of such products or manufacturers by the National Aeronautics and Space Administration.

Model 3 is a more refined version of Model 2 with 1,844,367 elements and 2,066,651 Nodes. The lateral mesh aspect ratio is 1.8 at the free edges and 4.6 in the middle. The mesh aspect ratio in the axial direction is 1.8 in the vicinity of the softening strip and 18.3 in the far-field region.

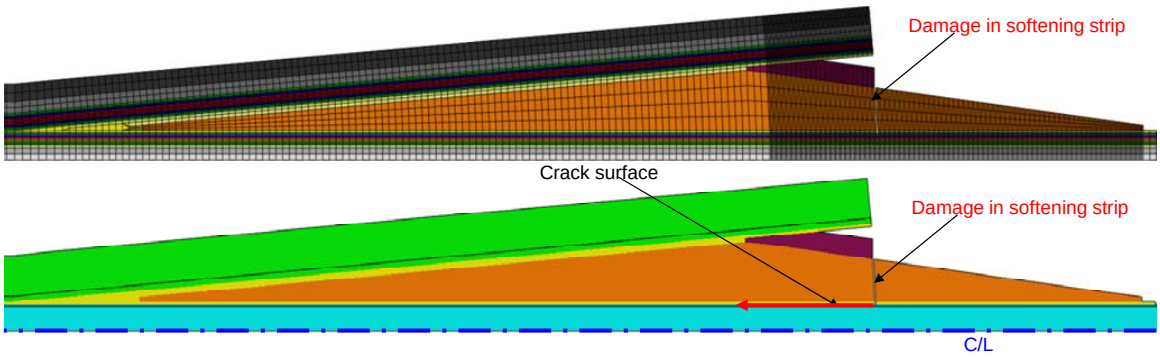

Figure 7. Model 2.

III. Test and Analysis Correlation

In this section, the results of several FE analyses of the y-joint specimen are presented. First, an undamaged FE model is compared with strain gage results. Modification of the material properties due to uncertainty is used to improve the initial correlation. Next, to account for a non-linear reduction in load capability near a strain gage and to further improve correlation, cracks are initiated at different locations in the FE model. Finally, an improved correlation is presented and a most likely failure scenario is presented.

A. Baseline FE analysis

Strain gage data from test PPY-1-B are plotted as solid lines in Figure 8. In the experimental test, the strain gages were set to zero after the specimen had been cooled to cryogenic temperatures at zero applied load. In Figure 8, the applied tensile load is normalized by the average failure load from the three experimental tests. Of the five strain gages plotted in Figure 8, gages 7 and 8 are back-to-back strain gages on the outer adherend surface in the far field region, gages 3 and 4 are back-to-back strain gages on the outer adherend surface in the softening strip region, and gage 2 is on the inner adherend surface in the far field region as shown in the cartoon in Figure 8. The back-to-back strain gages are close. The far-field strains (gages 2, 7, and 8) exhibit linear behavior while the softening strip strains (gages 3 and 4) exhibit non-linear behavior. Finite element strains from a geometrically nonlinear analysis of Model 1 are plotted in Figure 8 as dashed lines. The analytical strains do not match the strain gage values closely, especially in the softening strip region. In Figure 8, strains are normalized by the value of strain gage 3 at failure.

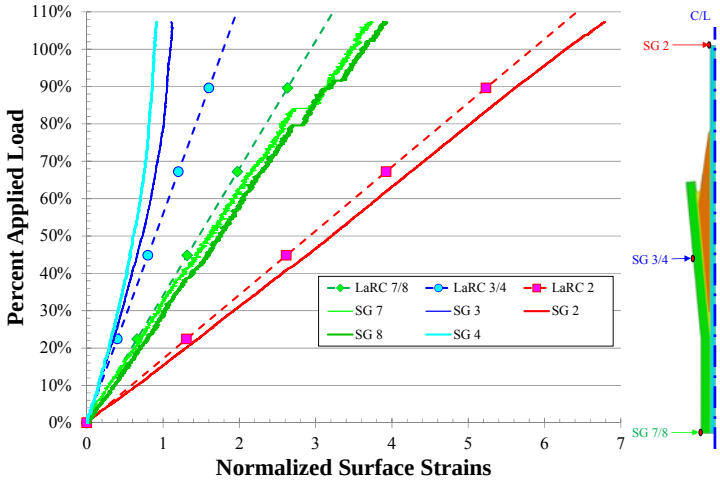

Figure 8. Comparison of LaRC FE results to PPY-1-B strain gages.

To compare the analytical strains to the strain gages from all three tests, Figure 9 was generated. In Figure 9, the percent difference in the strain gage measurements and the finite element results are plotted at six applied load values. Variation in the strain gage measurements among the three tests is approximately five percent. According to Figure 9, the analytical model is stiffer than the specimen in the far-field regions and more compliant than the specimen in the softening strip region. Analytical far-field strains in the FE were 10% lower than the strain gages (2, 7, and 8). This 10% difference is constant throughout the loading, and can be attributed to factors such as variation in material properties between the model and the specimen or differences in the thermal expansion properties of the strain gages and the specimen. Differences between the analytical strains and the strain gages (3 and 4) in the softening strip region were non-linear, increasing from 15% at low load to 80% at failure. The non-linear strain gage response in the vicinity of the softening strip indicates a reduction in the load carrying capability of the material in this region. The most likely cause of this non-linear effect is propagation of a crack, ultimately leading to complete delamination in the top plies of the inner adherend from the softening strip to the grips.

Because the differences in the analytical strains and the strain gages appear to be due to two different causes, two approaches must be used to match the analytical and test strains. First, the material properties of the FE model are adjusted to improve correlation in the far-field region, as discussed in Section III B below. Next, the delamination observed in the tests is included in the FE model. In Section III C, using delamination growth in the FE model to improve model correlation is discussed.

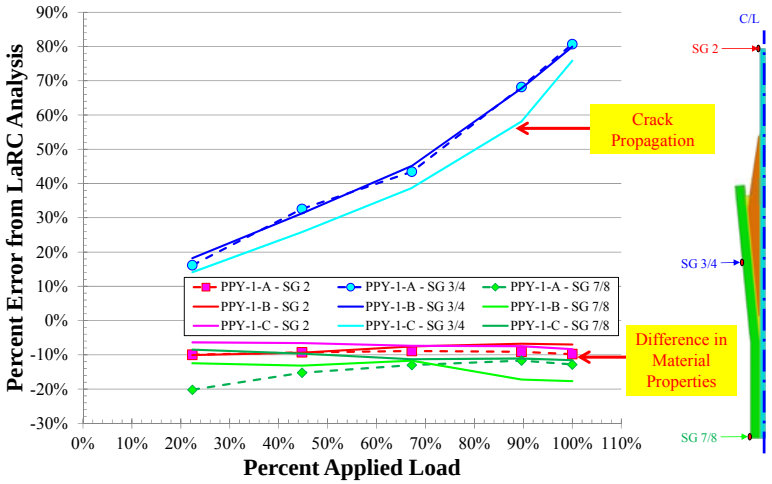

Figure 9. Percentage comparison of LaRC (Langley Research Center) FE results to PPY-1-A, B, and C strain gages.

B. Correlation of Far-Field Strains

The difference in the far-field strains could be attributed to several factors such as differences in the elastic properties of the specimen when compared to the baseline elastic property values due to inherent uncertainty. The differences could also be due to a mismatch in the thermal expansion coefficients of the strain gages and the specimen. In either case, the far-field strain predictions can be corrected by adjusting the material properties of the analytical model. An interpolation process is used with composite lamination theory (CLT, Ref. 4) to reduce the elastic modulus and match the experimental strain at failure. In this interpolation process, a reduction of the laminate modulus in the longitudinal fiber direction (E_L) by 8% was found to be sufficient to obtain the required strain. This modulus adjustment is applied to the FE model to produce the strains shown in Figure 10. In Figure 10, analytical strains now match the far-field strain gages (2, 7, and 8) but correlation with the gages (3 and 4) in the softening strip region has worsened.

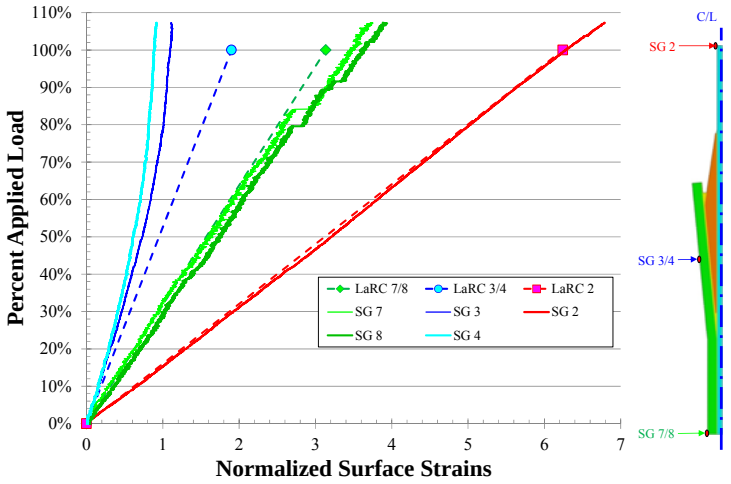

Figure 10. Comparison of LaRC FE results with modified properties to PPY-1-B strain gages.

C. Crack Initiation Studies

The nonlinearity in the strain gages in the softening-strip region is attributed to crack propagation (delamination) as observed in the specimens after failure. Delamination is replicated in Model 1 at a location corresponding to the delamination from the test, i.e. between the top two plies in the inner adherend from the softening strip to the grips. Nodes in the top surface are connected to the bottom surface using multi-point constraints (MPC). To introduce a crack, the MPCs in a selected region are deleted. During experimental testing, the specimens were encased in foam insulation and could not be visualized, so the exact initiation site for the crack is not known. To proceed with this analytical crack growth study, crack initiation is investigated at multiple locations.

For the first crack initiation study, the crack is assumed to initiate at the arrowhead (see Figure 6) and propagate toward the end of the softening strip. In Figure 11, the softening-strip zone strain at 100% load is plotted against increasing crack length. At a crack length of zero, the result from Figure 10 (about 1.9 times the strain gage measurement) is duplicated. As the crack grows from the arrowhead to the location of the tear in the softening strip from the test (about 3.2 in.), the strains are reduced to a normalized strain value of 1.3, but it does not reach the target value of 1.0. In order to match the strain gage value, the crack must be extended in the grip direction to a total length of over 5 in. However, this 5 in. crack reduces strains near the far-field gages (7 and 8) significantly, which is not consistent with the test data. Therefore, it is concluded that initiation of a crack at the arrowhead is unlikely.

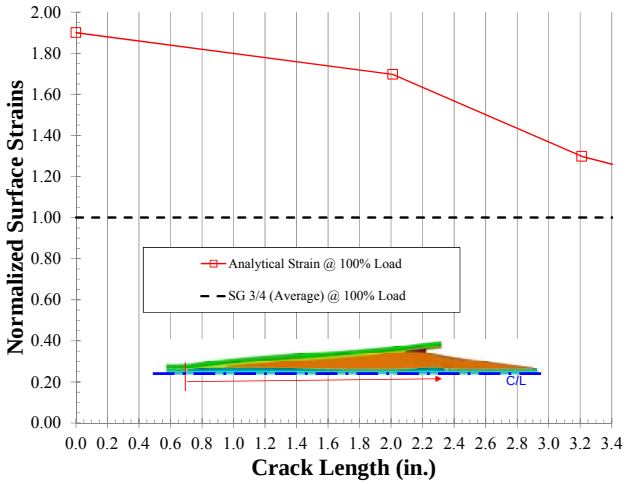

Figure 11. Crack propagation study, initiating at arrowhead.

For the second crack initiation study, the crack is assumed to initiate in the softening strip and propagate toward the grips. Crack propagation in the softening strip was not of interest, so a straight cut through the softening strip was modeled to represent the observed tear from the test specimens (see Model 2 in Figure 7). In Figure 12, the softening-strip zone strain in Model 2 at 100% load is plotted against increasing crack length. As shown in Figure 12, the analytical strain at 100% load reaches the target strain gage level at a crack length of 0.90 in. This crack growth study was repeated at five other load levels and matched to the corresponding strain gage values, as shown in Figure 13. In Figure 13, crack growth seems to be a nearly linear function of the applied load from load values of 20% to 100%. The crack length at the lowest load value (7%) in Figure 13 corresponds to a crack length of 0.4 in., and the curve does not seem to trend to a zero crack length at low load. Several factors can contribute to this apparent initial shift in the crack growth curve: softening strip damage during cryogenic cool down, differences in softening strip properties between the analytical model and the specimen, and inherent errors in strain gage readings at extremely low load.

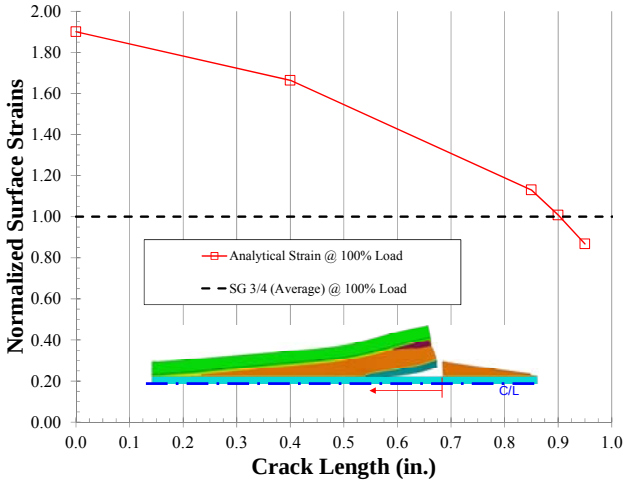

Figure 12. Crack propagation study, initiating at softening strip tear.

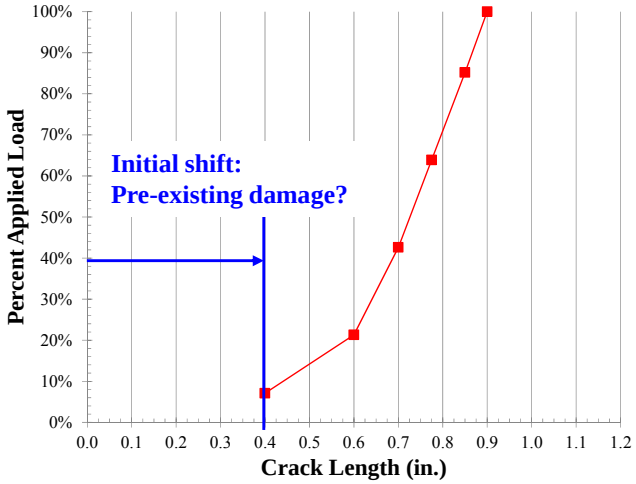

Figure 13. Applied load vs. crack length.

As shown in Figure 14, strains from the softening strip crack growth model (Model 2, including the E_L adjustment from section III B) correspond well with the experimental data. Of particular note is that the simulated cracks did not significantly affect the analytical strain results in the far-field region (gages 2, 7, and 8). Based on this crack growth study, the likely failure scenario for the PPY-1 specimens is that a crack initiated within the softening strip at a load value of less than 7% of the final failure load (as indicated by the initial shift in Figure 13).

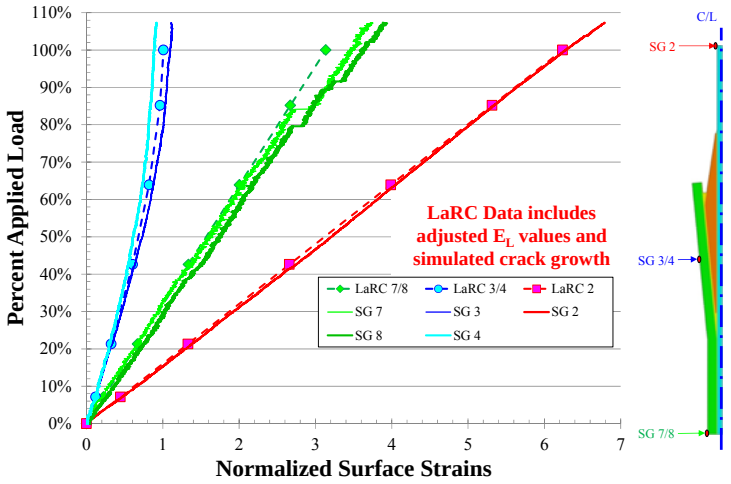

Figure 14. Comparison of LaRC FE results with modeled cracks to PPY-1-B strain gages.

IV. Fracture Mechanics Analysis

In this section, the results of a fracture mechanics analysis are presented. First, an overview of a commonly used fracture mechanics technique is presented. Next, results of a fracture mechanics study are presented. Finally, mesh convergence of the models used in the fracture mechanics study is discussed.

Linear elastic fracture mechanics (LEFM) has been a commonly used practice to characterize the onset and growth of delamination in composite structures for over three decades [Refs. 5-8]. Delamination is typically resolved into three failure modes: mode I due to interlaminar tension, mode II due to interlaminar sliding shear, and mode III due to interlaminar scissoring shear as shown in Figure 15. One widely used LEFM method called the virtually crack closure technique (VCCT) is used to compute the strain energy release rate (SERR) based on displacement and reaction force results from solid (3D) FE analyses.

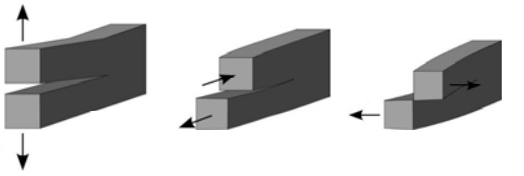

Mode I Interlaminar Tension | **Mode II** Interlaminar Sliding Shear | **Mode III** Interlaminar Scissoring Shear

Figure 15. Fracture modes.

As shown in Figure 16, SERR is computed for modes I, II, and III using Equations 1 to 3, respectively. In Equations 1 to 3, Δa is the length of the elements at the delamination front, and b is the width of the elements. Forces at the delamination front are X_{Li}, Y_{Li}, and Z_{Li}. Displacements behind the delamination at the upper face node are denoted, $u_{L\ell}$, $v_{L\ell}$, and $w_{L\ell}$. Displacements behind the delamination at the upper face node are denoted, $u_{L\ell^*}$, $v_{L\ell^*}$, and $w_{L\ell^*}$. In Equations 1 to 3, nodal displacements and reaction forces are obtained from the FE model.

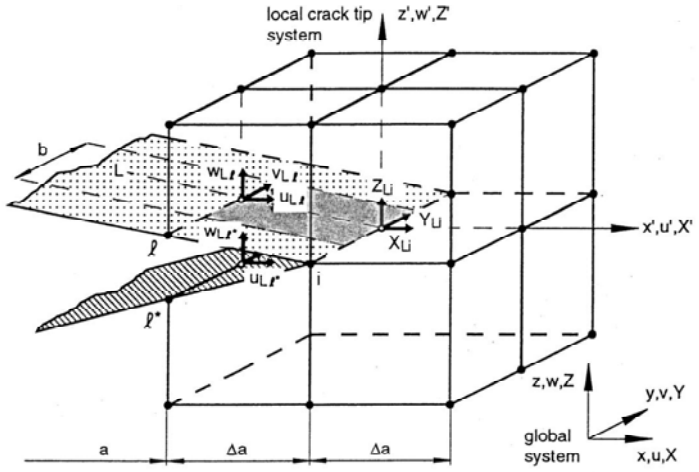

Figure 16. Virtual crack closure technique for eight-node solid elements.

$$G_I = -\frac{1}{2\Delta a\, b}\cdot\left(w_{L\ell} - w_{L\ell^*}\right)\cdot Z_{Li} \qquad (1)$$

$$G_{II} = -\frac{1}{2\Delta a\, b}\cdot\left(u_{L\ell} - u_{L\ell^*}\right)\cdot X_{Li} \qquad (2)$$

$$G_{III} = -\frac{1}{2\Delta a\, b}\cdot\left(v_{L\ell} - v_{L\ell^*}\right)\cdot Y_{Li} \qquad (3)$$

In Figure 17, total SERR ($G_T = G_I + G_{II} + G_{III}$) is plotted against width-wise position along the crack front, where y/b = 0 corresponds to the middle of the specimen. In Figure 17, G_T is normalized by the average mode I fracture toughness of the laminate. Five different crack fronts are plotted in Figure 17; each front corresponds to a different crack length and applied load. Total SERR increases with increasing load in the specimen.

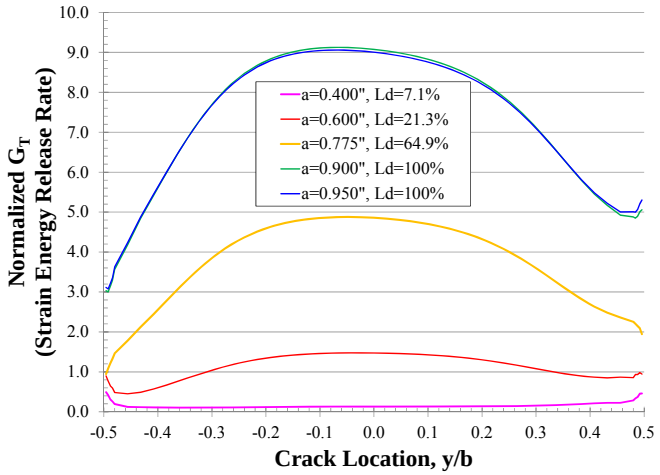

Figure 17. Total strain energy release rate as a function of width at various crack lengths.

In Figure 18, SERR is plotted against crack length at a constant load (100% of the average specimen failure load) in the middle of the specimen (y/b=0). As shown in Figure 18, mixed-mode delamination occurs at the crack front; SERR is approximately 70% mode I and 30% mode II. For a constant load, if G_T decreases with increasing

crack length, then crack growth is stable. Otherwise, there is no mechanism to arrest crack growth, and crack growth is unstable. The slope of G_T is flat in Figure 18, so crack growth at this location and load is unstable.

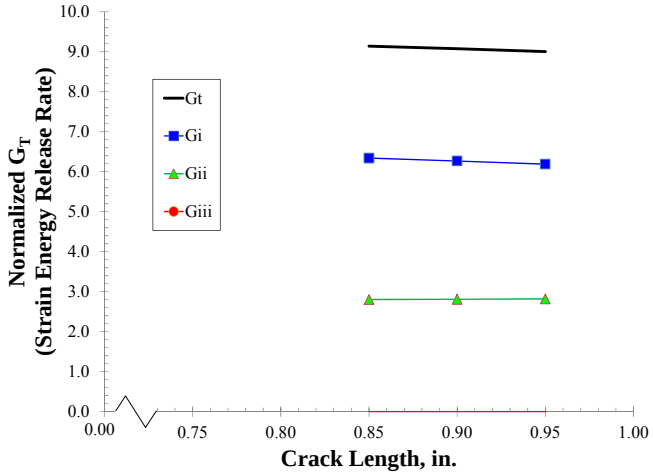

Figure 18. Strain energy release rate vs. crack length at y/b=0 and 100% load.

In Figure 19, SERR (modes I, II, and total) is plotted against width-wise position along the crack front for 100% load for two FE models: a coarse model (Model 2 from Section IIC) and a refined model. The mesh refinement in the softening strip region of the refined model is about 2.5 times the refinement of the coarse model, as previously discussed in Section IIC. The G_I/G_{II} mode mixity is slightly different between the coarse and refined models, but G_T is independent of mesh density.

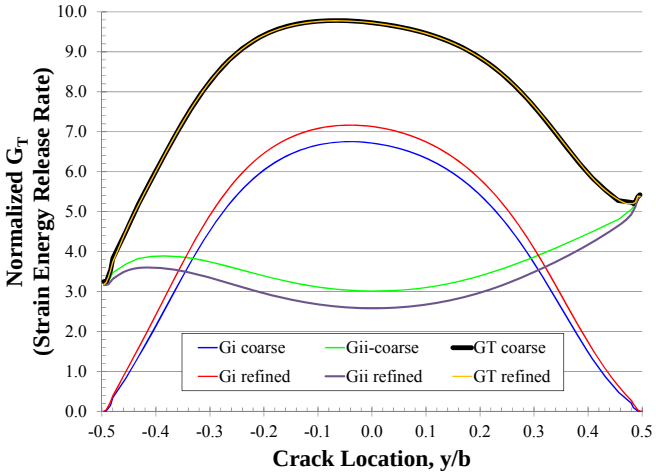

Figure 19. VCCT mesh refinement at 100% load.

V. Summary

The study presented in this paper correlated the analytical models with the test data for a y-joint test specimen. For the initial model used in this study, far-field strains differed by 10 to 20% from the strain gage readings. A simple 8% reduction in the elastic property values of the analytical model was sufficient to tune the finite element model strains to the strain gages. However, the analytical strains in the softening strip region of the specimen were inconsistent with the strain gage measurements. Nonlinearity in the strain gage behavior caused unloading of the angled skirt section in the softening strip region. It was necessary to model the delamination in the specimen to match the analytical strains in the softening strip region to the strain gages.

This paper established the most likely failure mode for the y-joint specimen. Based on the correlated finite element models, the most likely failure scenario is that delamination of the inner laminate of the specimen was precipitated by a crack in the softening strip. According to the analytical models, delamination began at below 20% of the failure load and propagated between the outermost two plies of the inner adherend all the way to the load grips. Another failure scenario was investigated: failure initiation at the adhesive arrowhead. This other failure scenario is considered highly unlikely because the analytical and test strains could not be correlated at the failure load without growing the crack to a length that adversely affected the far-field strains.

This paper demonstrated fracture mechanics methods on this test specimen. A limited amount of fracture toughness data were available, but mixed-mode toughness data were not available. With limited fracture toughness data and with no laminate strength data, progressive failure methods are not applicable to this problem. However, it is possible to evaluate crack stability using the virtual crack closure technique (VCCT). VCCT was applied to the analytical model of the specimen for various crack configurations. At the experimental failure load, the slope of strain energy release rate over crack length was flat, i.e. there is no mechanism to arrest crack growth. This unstable crack growth is consistent with the experimental failure load.

VI. References

[1]Sleight, David W., Martin, Robert A., and Johnson, Theodore F., "Structural Design and Sizing of a Metallic Cryotank Concept," 54th AIAA/ASME/ASCE/AHS/ ASC Structures, Structural Dynamics, and Materials Conference, Boston, MA, April 2013.

[2]Johnson, Theodore F., Sleight, David W., and Martin, Robert A., "Structures and Design Phase I Summary for the NASA Composite Cryotank Technology Demonstration Project," 54th AIAA/ASME/ASCE/AHS/ ASC Structures, Structural Dynamics, and Materials Conference, Boston, MA, April 2013.

[3]ABAQUS, *ABAQUS User's Manual*, Vol III, Version 6.12, Dassault Systèmes Simulia Corp., Pawtucket, RI, 2012.

[4]Jones, Robert M., *Mechanics of Composite Materials, Second Edition*, Taylor and Francis, Inc., Philadelphia, PA, 1998.

[5]Krueger, Ronald, "Virtual crack closure technique: History, approach, and applications," *Applied Mechanics Reviews*, Vol. 57, Issue 2, pp. 109-143, 26 April 2004.

[6]O'Brien, T. Kevin, "Characterization of delamination onset and growth in a composite laminate," *Damage in Composite Materials*, ASTM STP 775, American Society for Testing and Materials, Philadelphia, PA, pp. 140–167, 1982.

[7]O'Brien, T. Kevin, "Interlaminar fracture toughness: the long and winding road to standardization," *Composites, Part B: Engineering*, Vol. 29, Issue 1, pp. 57–62, 1998.

[8]Martin, R. H., "Incorporating interlaminar fracture mechanics into design," *International Conference on Designing Cost-Effective Composites*, IMechE Conference Transactions, London, U.K, pp. 83–92, 1998.

REPORT DOCUMENTATION PAGE

Form Approved
OMB No. 0704-0188

1. REPORT DATE *(DD-MM-YYYY)*	2. REPORT TYPE	3. DATES COVERED *(From - To)*
01- 10 - 2015	Technical Memorandum	

4. TITLE AND SUBTITLE

Test and Analysis Correlation for a Y-Joint Specimen for a Composite Cryotank

5a. CONTRACT NUMBER

5b. GRANT NUMBER

5c. PROGRAM ELEMENT NUMBER

6. AUTHOR(S)

Mason, Brian H.; Sleight, David W.; Grenoble, Ray W.

5d. PROJECT NUMBER

5e. TASK NUMBER

5f. WORK UNIT NUMBER

284848.02.05.07.01

7. PERFORMING ORGANIZATION NAME(S) AND ADDRESS(ES)

NASA Langley Research Center
Hampton, VA 23681-2199

8. PERFORMING ORGANIZATION REPORT NUMBER

L-20594

9. SPONSORING/MONITORING AGENCY NAME(S) AND ADDRESS(ES)

National Aeronautics and Space Administration
Washington, DC 20546-0001

10. SPONSOR/MONITOR'S ACRONYM(S)

NASA

11. SPONSOR/MONITOR'S REPORT NUMBER(S)

NASA-TM-2015-218967

12. DISTRIBUTION/AVAILABILITY STATEMENT

Unclassified - Unlimited
Subject Category 24
Availability: NASA STI Program (757) 864-9658

13. SUPPLEMENTARY NOTES

14. ABSTRACT

The Composite Cryotank Technology Demonstration (CCTD) project under NASA's Game Changing Development Program (GCDP) developed space technologies using advanced composite materials. Under CCTD, NASA funded the Boeing Company to design and test a number of element-level joint specimens as a precursor to a 2.4-m diameter composite cryotank. Preliminary analyses indicated that the y-joint in the cryotank had low margins of safety; hence the y-joint was considered to be a critical design region. The y-joint design includes a softening strip wedge to reduce localized shear stresses at the skirt/dome interface. In this paper, NASA-developed analytical models will be correlated with the experimental results of a series of positive-peel y-joint specimens from Boeing tests. Initial analytical models over-predicted the experimental strain gage readings in the far-field region by approximately 10%. The over-prediction was attributed to uncertainty in the elastic properties of the laminate and a mismatch between the thermal expansion of the strain gages and the laminate. The elastic properties of the analytical model were adjusted to account for the strain gage differences. The experimental strain gages also indicated a large non-linear effect in the softening strip region that was not predicted by the analytical model. This non-linear effect was attributed to delamination initiating in the softening strip region at below 20% of the failure load for the specimen.

15. SUBJECT TERMS

Cryotank; Failure; Game changing; Mathematical code; Softening

16. SECURITY CLASSIFICATION OF:			17. LIMITATION OF ABSTRACT	18. NUMBER OF PAGES	19a. NAME OF RESPONSIBLE PERSON
a. REPORT	b. ABSTRACT	c. THIS PAGE			STI Help Desk (email: help@sti.nasa.gov)
					19b. TELEPHONE NUMBER *(Include area code)*
U	U	U	UU	18	(757) 864-9658